A novel wavelet-based multi-resolution skeleton extraction from a moiré image

Chien-Yue Chen[1]*, Wing-Kwong Wong[1]**, Tsung-Lun Lin[1], Ching-Huang Lin[2]

[1]Institute of Electronic Engineering, National Yunlin University of Science & Technology, Yunlin, TAIWAN

[2]Department of Electrical Engineering, Hwa Hsia Institute of Technology, Taipei, TAIWAN

*chencyue@yuntech.edu.tw **wongwk@yuntech.edu.tw

Abstract: - The measuring of the surface altitude of a body with shadow moiré results in an image of contour lines. These contour lines are usually thick and can be broken at a number of places. A one-pixel wide skeleton of the image can be extracted by thresholding and thinning, which is a traditional approach in previous research. This study proposes a novel method based on wavelet transformation with multi-resolutions and object point detection. In particular, this method solves the problem of uneven lighting on the surface of the object and generates a clear binary image of unbroken contour lines of single-pixel width.

Key-Words: - Shadow moiré, contour recognition, wavelet transform, image processing

1 Introduction

Moiré, an image of contour lines, is generated by overlapping two grating with similar periods. These grating must be placed with transparent and opulent contours with equi-distance spacing [1]. Moiré images are common in daily life, e.g., textile and silk with grid patterns [2]. If parallel light rays through reference grating are projected on an object, a group of transformed shadows will be formed on the object's surface, based on the heights of various locations on the surface. These shadows overlap to form an image of non-overlapped lines called shadow moiré. With the computation according to a formula, each pair of neighboring non-overlapped lines differ by a constant height [3]. In other words, the lines form a contour map. Using the technology of optical moiré, one can measure the altitude contours of the surface of an object. In the last decade, the maturation of this technology has resulted in many industrial and scientific applications. This technology can detect the tiny change, which is difficult to detect visually, of the altitude of the surface of an object and magnify the tiny change to a visible scale. This is done without focusing on any local area so that the change of the entire surface can be viewed globally at the same time [4, 5].

In the 1970's, shadow moiré was first applied to detecting the tiny change in the altitude of the surface of a human body. The contour lines can show the change of the curvature of a patient's vertebrate [6]. Another application is the measurement of the change of the undulating surface above a muscle of interest [7]. Moiré shadow can also be used to record the tiny change of the surface radius artery of the right hand of a patient [8]. When a shadow moiré is formed on the surface of an object, a researcher often needs to detect whether a pattern of interest is found in the image of shadow moiré. This task can be automated if the image, which in its raw form usually consists of thick and sometimes overlapping or broken contours, can be simplified to just the skeleton, which should be sufficiently thin, of the image. An ideal skeleton image is a binary image with a black skeleton on a white background. In short, it is important to compute at skeleton from a raw contour map.

One common method of deriving a binary image from a gray-level image is called bilevel thresholding, which uses the statistical method of a gray-level histogram. Otsu [9], Kittler and Illingworth [10] use such a method but there are a few problems. One problem is its computational time complexity. Moreover the method does not work well for images where the light intensities are not evenly distributed. This problem originates from the way the image is produced. Usually, the image is obtained with a light source projected on the object at an angle. Some locations of the object get more light and others get less, resulting in an uneven distribution of the gray level in the light parts as well as in the dark parts of the image. One solution

to this problem is to partition the image into various locations based on the gray level of the locations and then use multilevel thresholding instead of bilevel thresholding. Otsu [11] extends bilevel thresholding to multilevel thresholding, resulting in more efficient algorithms [12]. Other researchers propose algorithms based on the entropy theorem [13-15]. Methods based on other mathematical models are also proposed [16-21].

A binary moiré image whose contours are one-pixel wide can show the skeletal pattern of the image clearly, allowing accurate measurement of the surface altitude. Thinning algorithms are commonly used for this task, as the geometric features of the skeleton are preserved after thinning [22]. Various thinning algorithms are presented in [23] and the importance of the time complexities of these algorithms for image processing applications are discussed in [24]. Applications include the recognition of language symbols, geometric shapes, or finger prints [25-28]. Skeleton extraction can also be done with a pulse coupled neural network [29].

2 Novel method of skeleton extraction

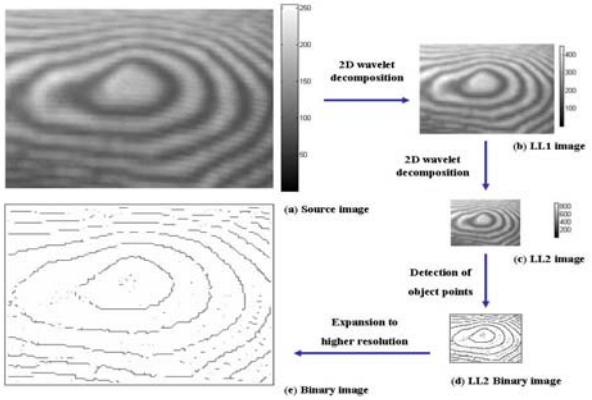

Fig. 1. A novel method of skeleton extraction with DWT

Previous research often applies two stages of thresholding and then thinning to extract a thin skeleton of a moiré image. We propose a novel method to solve the same problem. Our method addresses the problem of uneven distribution of gray level in the image and produces a skeleton of single-pixel width. The method is summarized in Figure 1. First, the 2D wavelet decomposition of the source moiré image produces an approximation LL1 image with half of the original size for each dimension. Then the same process is applied to the LL1 image, producing an LL2 image with a quarter of the original size for each dimension. In the LL2 image, the object points of the skeleton are detected, resulting in one-pixel wide contour lines that form the skeleton of the dark parts of the image. Finally, the skeleton image is expanded back to the size of the original image. Each of the steps will be explained as figure 1.

2.1 Discrete wavelet transform in two dimensions

Discrete wavelet transform (DWT) can provide relative resolution depending on the frequency spectrum of a given signal. In Eq. (1), With good choices of a mother wavelet function and a scale function, the DWT of function $f(x) \in L^2(R)$ is defined relative to wavelet $\psi(x)$ and scaling function $\varphi(x)$ in one dimension. This j_0 is an arbitrary starting scale and 2^J of data size is selected such that the summations are performed over $x = 0,1,2,...,M-1$, $j = 0,1,2,...,J-1$, and $k = 1,2,...,2^j - 1$. Eq. (2) is normally called the approximation or scaling coefficients; the Eq. (3) is referred to as the detail or wavelet coefficient.

$$f(x) = \frac{1}{\sqrt{M}} \sum_k W_\varphi(j_0,k)\varphi_{j_0,k}(x) + \frac{1}{\sqrt{M}} \sum_{j=j_0}^{\infty} \sum_k W_\psi(k)\psi_{j,k}(x) \quad (1)$$

$$W_\varphi(j_0,k) = \frac{1}{\sqrt{M}} \sum_x f(x)\varphi_{j_0,k}(x) \quad (2)$$

$$W_\varphi(j,k) = \frac{1}{\sqrt{M}} \sum_x f(x)\psi_{j,k}(x) \quad (3)$$

The application of DWT to an image can extent form one-dimension to two-dimension. A two-dimensional scaling function $\varphi(x,y)$ and three two-dimensional wavelets, $\psi^H(x,y)$, $\psi^V(x,y)$, and $\psi^V(x,y)$, are required in two dimensions. Each is the product of a one-dimensional scaling φ function and corresponding wavelet ψ, produce four products of separable scaling function (show in Eq (4)) and separable directionally sensitive wavelet [show in Eq (5~7)]. These wavelets measure functional variations in intensity or gray-level variation for image, along different directions. ψ^H measure variations along columns (for example, horizontal edges), ψ^V responds to variations along rows (for example, vertical edges), and

ψ^D corresponds to variations along diagonals. We normally let $j_0 = 0$, $m = 1,2,...,2^j - 1$ and $n = 1,2,...,2^j - 1$. Wavelet transform of function $f(x,y)$ of size $M \times N$ is then given by Eq. (8). The $W_\varphi(j_0,m,n)$ coefficients define an approximation of $f(x,y)$ at scale j_0. The $W_\psi{}^i(j,m,n)$ coefficients add horizontal, vertical, and diagonal details for scales $j \geq j_0$

$$\varphi(x,y) = \varphi(x)\varphi(y) \tag{4}$$

$$\psi^H(x,y) = \psi(x)\varphi(y) \tag{5}$$

$$\psi^V(x,y) = \varphi(x)\psi(y) \tag{6}$$

$$\psi^D(x,y) = \psi(x)\psi(y) \tag{7}$$

$$\begin{aligned} f(x,y) &= \frac{1}{\sqrt{MN}} \sum\sum W_\varphi(j_0,mn)\varphi_{j0,m,n}(x,y) \\ &+ \frac{1}{\sqrt{MN}} \sum_{i=H,V,D_0} \sum_{j=j_0}^{\infty} \sum\sum\sum W_\Psi^i(j,m,n)\Psi^i_{j,mn}(x,y) \end{aligned} \tag{8}$$

The two-dimensional DWT can be implemented using digital filters and downsamplers. The image $f(x,y)$ is used as the $W_\varphi(J,m,n)$ input. The sing-scale filter bank of Figure 2 can be iterated by tying the approximation output to the input of another filter bank. Convolving its rows with $h_\varphi(-n)$ and $h_\psi(-n)$ and downsampling its columns, we get two subimages whose horizontal resolutions are reduced by a factor of 2. The highpass or detail compont characterizes the image's high-frequency information with vertical; the lowpass, approximation component contains its low-frequency, vertical information. Both subimages are then filtered columnwise and downsampled to yield four quarter-size output subimages: W_φ, $W_\psi{}^H$, $W_\psi{}^V$ and $W_\psi{}^D$ [30].

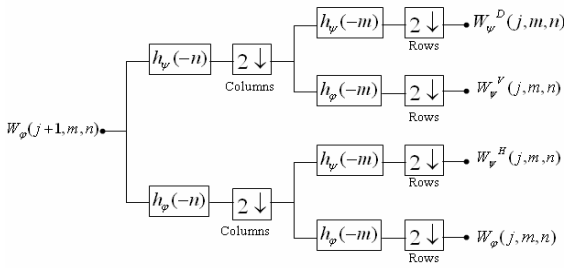

Fig. 2. The analysis filter bank

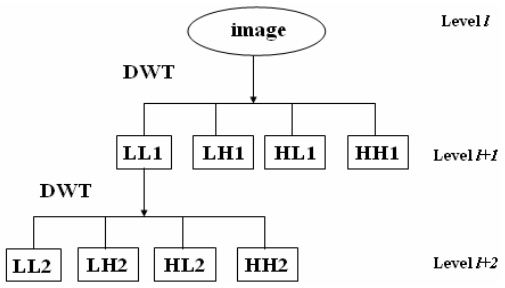

Fig. 3. Hierarchical system of 2D DWT

2.2 Detection of object points with multi-resolution

DWT, as a hierarchical system, has the property of multiple analytical resolutions (Figure 3). The application of a multi-level two-dimensional wavelet transform to an M*N image at level l results in four sub-images, each of M/2*N/2, at level l+1. LL1 is a coarse approximation of the original image, while LH1, HL1, and HH1 show finer details (Figure 3). Similarly, LL1 at level l+1 can be partitioned into four sub-images, each of M/4*N/4, at level l+2 [31]. Another study applies this method to the edge detection of a given image [32]. The application uses a sliding window searching and tracking for object points that are discontinuous (Figure 4). It makes uses of the association of points between two levels.

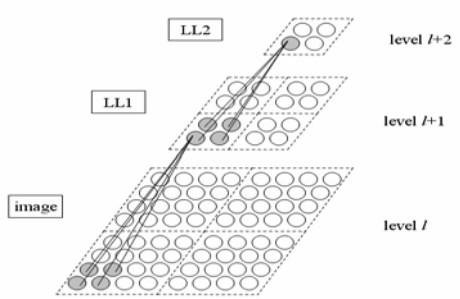

Fig. 4. Relation between the levels of point to point

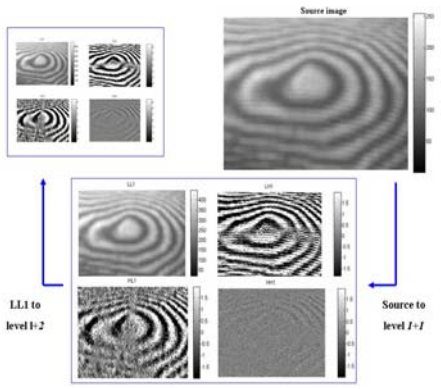

Fig. 5 Multi-resolution DWT decomposition of image

This study proposes to apply a similar idea to derive a binary image from a moiré image. We use Haar as the mother wavelet with parameters -0.7071 and 0.7077. The visual meanings of the resulting DWT hierarchical images is shown in Figure 5. The method makes use of the original image, the LL1 image and the LL2 image at three different levels. Each image at a lower level is obtained by shrinking the image at an upper level by a factor of two for each dimension while preserving the characteristics of the original image. Given a gray level image of M*N resolution, our method detects object points in the image and derive a number of LL2 images at level l+2 with resolution M/4*N/4. Let (x,y) be the coordinates of a pixels in an LL2 image. Then a, b, c, d, e, f, g and h are the neighbor points of s in a window of 3*3, where s is the center of the window (Figure 6). Let V(p) be the gray level of point p. Consider the four conditions from (9) to (12):

$$\big(V(a) > V(s)\big) \& \big(V(e) > V(s)\big) \qquad (9)$$

$$\big(V(c) > V(s)\big) \& \big(V(g) > V(s)\big) \qquad (10)$$

$$\big(V(b) > V(s)\big) \& \big(V(f) > V(s)\big) \qquad (11)$$

$$\big(V(h) > V(s)\big) \& \big(V(d) > V(s)\big) \qquad (12)$$

If any two of the four conditions are satisfied, then s is an object point.

a (x-1,y+1)	**b** (x,y+1)	**c** (x+1,y+1)
h (x - 1 , y)	**s** (x , y)	**d** (x + 1 , y)
g (x-1,y-1)	**f** (x,y-1)	**e** (x+1,y-1)

Fig. 6. Neighbor points of pixels

Corner point	Neighbor on row	Neighbor on column
a	*b*	*H*
c	*b*	*D*
e	*f*	*D*
g	*f*	*H*

Table. 1 Neighbors of corner points

2.3 Expansion of the skeleton image of LL2 back to the original size

The skeleton image of the LL2 image is only a quarter of the size of the original image for each dimension (Figure 1e). Therefore, it is necessary to expand the skeleton image back to its original size. Consider an object point s in the image at level l+2, its eight neighbor points include a, b, c, d, e, f, g and h. Whether they are also object points at level l+2 will affect the sixteen points associated with s at level l. If the top neighbor b of s is also an object point, then the top two pixels of the third column are both object points at level l (Figure 7a). If the right neighbor d of s is also an object point, then the two rightmost pixels of the second row are both object points at level l (Figure 7b). If the bottom neighbor of s is also an object point, then the bottom two points of the third column are also object points at level l (Figure 7c). If the left neighbor h of s is also an object point, then the two leftmost points of the second row are object points at level l (Figure 7d). The union of the object points obtained with these four rules results in a set S1.

Next consider the four corner neighbors of s. If the top left neighbor a of s is also an object point, then the top left half of the diagonal are also object points at level l (Figure 8a). For the other three corner neighbors c, e, and g, the rules work similarly (b, c, d of Figure 8). The application of the above eight rules to the LL2 image at level l+2 will result in an image of M*N at level l. The object points of this image are assigned the gray level of 0 while the remaining, non-object points are assigned the gray level of 255. The result is a binary image of the original size, with thin lines of single-pixel width and is a rough skeleton of the original image.

The number of object point of the sub-image LL2 at level l+2 is 1/16 of that of the original image at level l. Using the above criteria for picking out the object points, the method obtains a new binary image with size $M/4 \times N/4$. Each point of LL2 corresponds to four points at level l+1 and to sixteen points at level l+2. LL2 can be considered a rough representation of the original image shrunk to a quarter of its size on each dimension. Therefore, the image at LL2 should be expanded back to its original size of M*N. A straightforward expansion will result in two conditions for the contours. First, the curvatures of the resulted contours are not smooth. Second, many contour lines are often more than one pixel wide. In order to solve these two problems, we use several simple expansion rules.

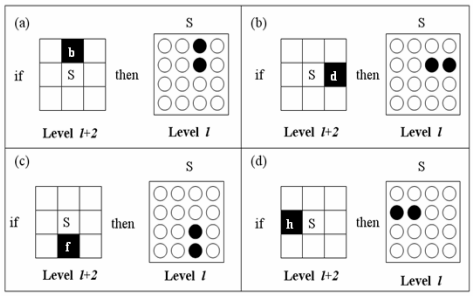

Fig. 7. Rules for adding object points at level l depending on the pattern out level l+2 (a) Top neighbor b is also an object point (b) Right neighbor d is also an object point (c) Bottom neighbor f is also an object point (d) Left neighbor h is also an object point

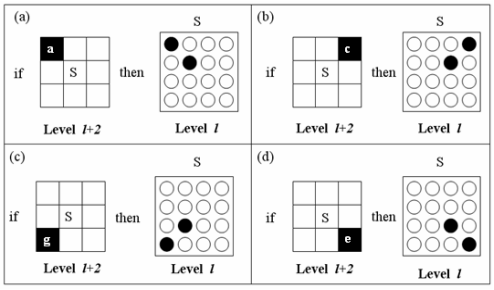

Fig. 8. Rules for adding object points at level l depending on the pattern out level l+2 (a) Top left neighbor a is also an object point (b) Top right neighbor c is also an object point (c) Bottom right neighbor g is also an object point (d) Bottom left neighbor e is also an object point

3 Implementation and discussion

This study makes use of the method of shadow moiré (Figure 9) [8]. Shadow moiré is projected on the surface of the test object. In order to increase the contrast of the shadow moiré, a special material is painted on the object. A Sony Digital Video camera captures the image of the shadow moiré. Above the test object and closer to the light source than the camera is a reference grating, which is Ronchi ruling grating of period P. Parallel light rays pass through the reference grating and project on the object with angle α (Figure 10). A grating shadow is produced on the surface of the object. Overlapping the reference grating and the transformed shadow will produce a number of alternating shadow stripes. Different contour patterns will result depending on the heights of various locations on the surface of the object. The camera will capture the image of the contours at angle β. Neighbor stripes differ by a constant height. Consider the Nth contour line. The difference between the height of this line and the reference grating is h [3]:

$$h = \frac{NP}{\tan\alpha + \tan\beta} \tag{13}$$

When we capture the image with a CCD, the altitude of the grating, its horizontality, the focus distance of the CCD affect the evenness of the distribution of the background light projected on the object. Shadow moiré is a light pattern produced by overlapping the reference grating and the transformed shadow. What a researcher wants to get is the shadow pattern of the transformed surface of the test object. The shadow pattern of the grating is not desirable. This unwanted shadow can be decreased by moving the grating relative to the test object. Ideally, this can reduce the intensity of the unwanted shadow and the background light. But in practice, the image captured in experiment contains visible traces of the grating pattern.

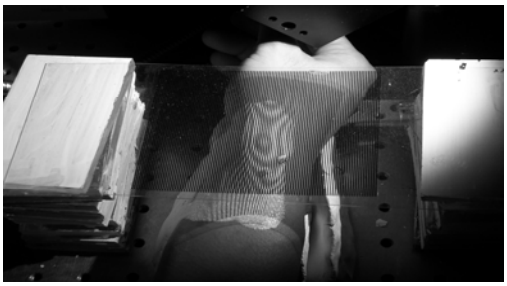

Fig. 9. Projection moiré on a wrist

Our test object is part of the wrist covering the main artery. A sample shadow moiré image of size 512*384 is shown in Figure 11a. The image is a bit twisted, with expanding, alternating stripes. Each stripe is a contour line of constant height. The surface can be a hill with increasing height at the center or a valley with decreasing height at the center. Figure 11a is obtained with Otsu's method of bilevel thresholding [9]. Figure 11b is obtained by maximizing the between-class variance of gray-level histogram and then by thresholding. Using bilevel threshold value cannot show the entire pattern clearly and evenly. In our experiments, we discover that the shadows at the bottom and close to the camera are overlapping, while the shadows at the top and close to the light source are thin and can disappear altogether. In short, there is an uneven distribution of gray level in the image and the method of bilevel thresholding will often produce a skeleton of low quality.

In order to address this problem, we use the method of multilevel thresholding. By dividing the gray-level image into different regions, we can solve the problem of uneven distribution of the background light intensity for the object image. Figure 11c shows the result of applying our method to the original shadow moiré image of Figure 11a. The result image, which is a big improvement in comparison to the image of Figure 11b, shows a

single-pixel wide skeleton of the original image with a few broken contours. In order to show the quality of the skeleton, we overlap the images of Figure 11a and 11c to produce Figure 11d.

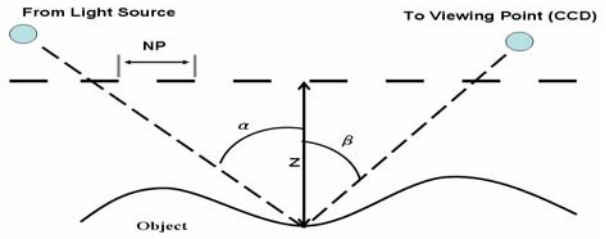

Fig. 10. Schematic diagram of shadow moiré pattern production

(a)

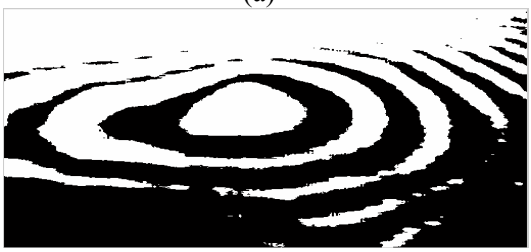

(b)

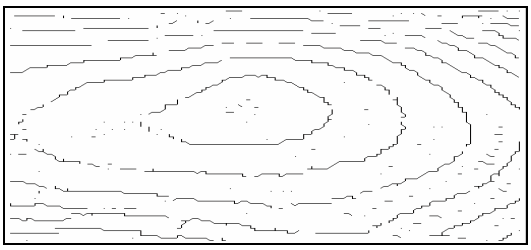

(c)

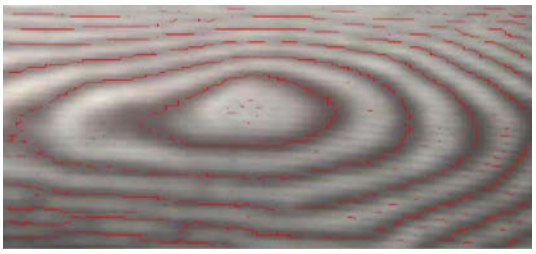

(d)

Fig. 11. (a) source moiré image (b) The binary image using Otsu's method (c) The binary image using our method (d) The image by overlapping (a) and (c).

4 Conclusion

In this study, we apply the technology of shadow moiré to capture the contour lines of the surface of the artery area of the wrist. The captured image of gray-level contains thick contours that are difficult to be recognized. Therefore, there is a need to extract the skeleton of the contours that is ideally single-pixel wide and the image should be binary rather than gray-level. A common method of skeleton extraction is bilevel thresholding which includes the stages of thinning and thresholding. This method suffers from the uneven distribution of background light on the object. In order to address this problem, we propose a novel method of applying wavelet transform to extract a skeleton of the image, resulting in a shrunken image of one quarter of the original size. Then the shrunken skeleton is expanded back to its original size with a few simple logic rules. The result is a much better binary skeleton that is single-pixel wide for each of the contour lines. The skeleton can be used to produce a much better estimate of the altitudes of various locations on the surface of the test object. With a number of contour maps taken continuously, a 3-D motion model of the surface can be generated. This is a future work we have in mind.

References:

[1] D. Post, and B. Han, High Sensitivity Moiré, New York, Springer-Verlag, 1994.
[2] I. Amidror, The theory of the moiré phenomenon, Kluwer Academic Publishers, Dordrecht, 2000.
[3] Kafri O., Glatt I., The Physics of Moiré Metrology, New York : Wiley, 1989, p.5-13.
[4] B. Han, D. Post, P Ifju, Moiré interferometry for engineering mechanics : current practices and future developments, The Journal of strain Analysis for Engineering Design, 36:101-117 (2001).
[5] B. Han, D. Post, P Ifju, Moiré Methods for Engineering and Science – Moiré Interferometry and Shadow Moiré, Topics in Applied Physics, 77:151 (2000).
[6] H. Takasaki, Moiré topography, Applied Optics, 19:1467-1472 (1970).
[7] R. S. Chang, C. Y. Lin, H. J. Shieh, A Study of behavior of a Muscle Pulsing with Phase Moiré

Imaging System, in Proceedings of the National Science Council, R.O.C (A), 20:1:64-69 (1996).
[8] C.Y. Chan, R.S. Chang, C.H. Lin C.D. Kuo , Pulse Measurement Based on Moiré Diagnostic System, WSEAS Transactions on System, 4:4:686-692 (2007).
[9] N. Otsu, A Threshold Selection Method from Grey-Level Histograms, IEEE Trans. Systems, Man, and Cybernetics, 9:1: 377-393 (1979).
[10] J. Kittler and J. lllingworth, Minimum Error Thresholding, Pattern Recognition, 19:41-47 (1986).
[11] S. S. Reddi, S. F. Rudin, H.R. Keshavan, An Optimal Multiple Threshold Scheme for Image Segmentation, IEEE Trans. System Man and Cybernetics, 14:4:661-665 (1984).
[12] P. S. Liao, T. S. Chen, P. C. Chung, A Fast Algorithm For Multilevel Thresholding, Journal of Information Science and Engineering, 17:5:713-727 (2001).
[13] M. S. and R. T., A new dichotomization technique to multilevel thresholding devoted to inspection applications, Pattern Recognition Letters, 21:2:151-161, February (2000).
[14] P. Y. Yin, Maximum entropy-based optimal threshold selection using deterministic reinforcement learning with controlled randomization, Signal Processing, 82:7:993-1006, July (2002).
[15] L. Cao, Z.K. Shi and E. K.W. Chenp, Fast automatic multilevel thresholding method, Electronics Letters, 38:16:868 - 870, Aug (2002).
[16] J. C. Yen, F.J. Chang, S. Chang, A new criterion for automatic multilevel thresholding, IEEE Transactions on mage Processing, 4:3:370-378, March (1995).
[17] P. Y. Yin and L. H. Chen, A fast iterative scheme for multilevel thresholding methods, Signal Processing, 60:3:305-313, August (1997).
[18] H. D. Cheng, C. H. Chen, H. H. Chiu, H. Xu, Fuzzy homogeneity approach to multilevel thresholding, IEEE Transactions on Image Processing, 7:7:1084- 1086, July (1998).
[19] S. H. Hamed, S. Reza, Automatic multilevel thresholding for image segmentation by the growing time adaptive self-organizing map, IEEE Transactions on Pattern Analysis and Machine Intelligence, 24:10:1388- 1393, Oct (2002).
[20] F. Murtagh, J. L. Starck, Quantization from Bayes factors with application to multilevel thresholding" Pattern Recognition Letters, 24:12:2001-2007, August (2003).
[21] E. Zahara, S. S. Fan and D. M. Tsai, Optimal multi-thresholding using a hybrid optimization approach, Patte Recognition Letters, 26:8:1082-1095, June (2005).
[22] Shu Changxian, Mo Yulong, Morphological thinning based on image's edges, International Conference on Communication Technology Proceedings, 1:5, Oct. (1998).
[23] L. Lam, S. Lee, C. Suen, Thinning Methodologies - A Comprehensive Survey, IEEE Trans. Pattern Analysis and Machine Intelligence, 14:9:869-885, Sept. (1992).
[24] W. N. Leung, C. M. Ng, P. C. Yu, Contour following parallel thinning for simple binary images, IEEE International Conference on Systems, Man, and Cybernetics, vol.3:1650-1655, Oct. (2000).
[25] Y. Kim, W. Choi, S. Kim, High-Speed Thinning Processor for Character Recognition System, IEEE Trans. Consumer Electronics, 38:4:762-766 (1992).
[26] Maher Ahmed, Rabab Ward, A rotation invariant rule-based thinning algorithm for character recognition, IEEE Transactions on Pattern Analysis and Machine Intelligence, 24:12:1672-1678, Dec. (2002).
[27] P. M. Patil, S. R. Suralkar, F. B. Sheikh, Rotation invariant thinning algorithm to detect ridge bifurcations for fingerprint identification, IEEE International Conference on Tools with Artificial Intelligence, 8, ICTAI 05. 17th, Nov. (2005).
[28] M. Tico, P. Kuosmanen, An algorithm for fingerprint image postprocessing, Conference Record of the Thirty-Fourth Asilomar Conference on Signals, Systems and Computers, 2:1735-1739, Oct. (2000).
[29] Xiaodong Gu, Daoheng Yu, Liming Zhang, Image thinning using pulse coupled neural network, Pattern Recognition Letters, 25:9:1075-1084, July (2004).
[30] R. C. Gonzalez, R. E. Woods, Digital Image Processing 2n
[31] M. S. Crouse, R. D. Nowak, R.G. Baraniuk, Wavelet-based statistical signal processing using hidden Markov models, IEEE Trans. Signal Process, 46:4:886–902 (1998).
[32] Ming-Yu Shih, Din-Chang Tseng, A wavelet-based multiresolution edge detection and tracking, Image and Vision Computing, 23:441-451 (2005).